Microporous and Mesoporous Materials 312 (2021) 110744

Contents lists available at ScienceDirect

Microporous and Mesoporous Materials

journal homepage: http://www.elsevier.com/locate/micromeso

Entropy in multiple equilibria. Argon and nitrogen adsorption isotherms of nonporous, microporous, and mesoporous materials

Gion Calzaferri [a,*], Samuel H. Gallagher [b], Dominik Brühwiler [b,*]

[a] Department of Chemistry and Biochemistry, Freiestrasse 3, 3012, Bern, Switzerland
[b] Institute of Chemistry and Biotechnology, Zurich University of Applied Sciences (ZHAW), 8820, Wädenswil, Switzerland

ARTICLE INFO

Keywords:
Adsorption
Isotherms
Zeolite L
MCM-41
Stöber-type silica
Entropy

ABSTRACT

Analysis of multiple equilibria of compounds with different coordination sites is extended to the description of adsorption isotherms with focus on the low relative pressure range. The entropy evolution is described using the particle distribution theory which also holds for adsorbents consisting of materials bearing more than one type of sites and applies for the condition that the adsorptive-adsorbent binding strength is larger than the adsorptive-adsorbate binding strength, so that monolayer coverage is favored. This allows to accurately determine the adsorption enthalpy. No assumption concerning the growth mechanism and specifics regarding the structure of the surface is needed. We find on a rigorous basis that this leads to Langmuir's equation for each site independently, that the total fractional amount of bound adsorptive can be described as a linear combination of individual Langmuir isotherms, and that such a linear combination has never the shape of the original Langmuir isotherms. The results are successfully applied to argon and nitrogen adsorption isotherms of nonporous, microporous, and mesoporous adsorbents which allows comparing systems for which the properties of the active surface span a large range. We observe that all experimental data can accurately be described by means of a linear combination of two Langmuir isotherms in the low relative pressure range up to a coverage of 60%–95%. This means that the shape of all adsorption isotherms is essentially determined by the entropy decrease with increasing coverage. The two site interactions involved exhibit substantially different adsorption enthalpies. Interestingly the Ar enthalpy of adsorption $\Delta_{ads}H_1^{\varnothing}$ of the sites 1 for the Stöber-type silica and of the three investigated MCM-41 adsorbents (with pore size of 2.7 nm, 4.1 nm, and 4.4 nm) are similar, namely −11 kJ/mol. The situation is analogous for the enthalpy of adsorption $\Delta_{ads}H_2^{\varnothing}$ for the sites 2, which amounts to −8 kJ/mol. A significantly larger enthalpy of adsorption $\Delta_{ads}H_1^{\varnothing}$ for the sites 1, namely −14.3 kJ/mol, and $\Delta_{ads}H_2^{\varnothing} = -11.7$ kJ/mol for the sites 2 is measured for potassium zeolite L thus reflecting the more polar nature of this adsorbent. The measured specific surface area for these samples ranges from 14 m^2/g for the Stöber-type silica up to 1100 m^2/g for the MCM-41(4.1 nm) adsorbent. The information provided by the lc2-L (linear combination of 2 Langmuir functions) analysis allows calculating the evolution of the coverage of site 1 and of site 2 as a function of increasing pressure. The inflection points of the isotherms, which mark the point where the curvature changes sign, were determined by numerically evaluating the second derivatives which vanish at this point and are compared with values obtained using BET analysis.

1. Introduction

Irving Langmuir mentioned already in 1918 that a surface can consist of different kinds of sites and that the isotherms should in such cases be described as a linear combination of individual isotherms [1]. It took some time before this suggestion was discussed and, as a consequence, used successfully to describe systems consisting of several sites with different ease of adsorption and for multi-component gas analysis. These descriptions are often abbreviated as DSL for dual-site Langmuir or DPL for dual-process Langmuir [2–18]. We showed how the free reaction enthalpy in multiple equilibria can be split into the particle distribution term and all other contributions for each type of sites separately, which allows to evaluate the entropy contribution [19]. A result of this analysis is that the fractional equilibrium coverage of the sites can be described

* Corresponding author.
E-mail addresses: gion.calzaferri@dcb.unibe.ch (G. Calzaferri), dominik.bruehwiler@zhaw.ch (D. Brühwiler).

https://doi.org/10.1016/j.micromeso.2020.110744
Received 25 July 2020; Received in revised form 2 October 2020; Accepted 29 October 2020
Available online 6 November 2020

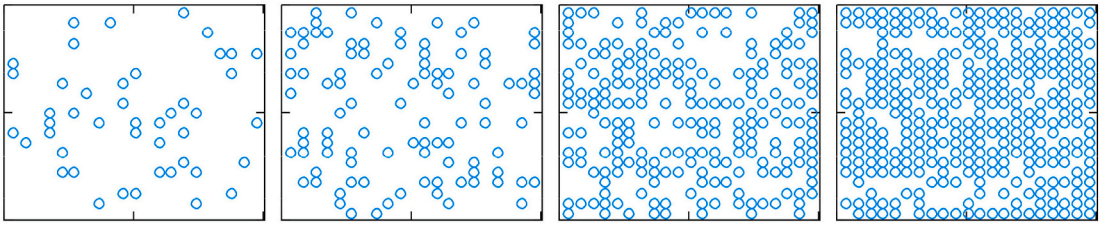

Fig. 1. Monte Carlo simulation showing the occupation of equally distributed adsorption sites from left to right for 10%, 25%, 50%, and 75% coverage. The circles show particles that have been adsorbed. Calculations were performed for 15,000 adsorbent sites. The figure shows a section of 20x20 equally distributed adsorbent sites. (For interpretation of the references to color in this figure legend, the reader is referred to the Web version of this article.)

Table 1
Adsorption equilibria of adsorptive *X* with different sites *A,B,C* etc of the adsorbent.

Equilibria	Equilibrium constants[a),b)]	
$\{X_{\rho c_A-1}A\}\{X_{rc_B}B\}\{X_{rc_C}C\}etc + X \rightleftarrows \{X_{\rho c_A}A\}\{X_{rc_B}B\}\{X_{rc_C}C\}etc$	$K^A_{\rho c_A, rc_B, rc_C \ldots} = \frac{[\{X_{\rho c_A}A\}\{X_{rc_B}B\}\{X_{rc_C}C\}etc\,]c^{\varnothing}}{[\{X_{\rho c_A-1}A\}\{X_{rc_B}B\}\{X_{rc_C}C\}etc][X]}$	(1)
$\{X_{rc_A}A\}\{X_{\rho c_B-1}B\}\{X_{rc_C}C\}etc + X \rightleftarrows \{X_{rc_A}A\}\{X_{\rho c_B}B\}\{X_{rc_C}C\}etc$	$K^B_{rc_A, \rho c_B, rc_C \ldots} = \frac{[\{X_{rc_A}A\}\{X_{\rho c_B}B\}\{X_{rc_C}C\}etc\,]c^{\varnothing}}{[\{X_{rc_A}A\}\{X_{\rho c_B-1}B\}\{X_{rc_C}C\}etc][X]}$	(2)
$\{X_{rc_A}A\}\{X_{rc_B}B\}\{X_{\rho c_C-1}C\}etc + X \rightleftarrows \{X_{rc_A}A\}\{X_{rc_B}B\}\{X_{\rho c_C}C\}etc$	$K^C_{rc_A, rc_B, \rho c_C \ldots} = \frac{[\{X_{rc_A}A\}\{X_{rc_B}B\}\{X_{\rho c_C}C\}etc\,]c^{\varnothing}}{[\{X_{rc_A}A\}\{X_{rc_B}B\}\{X_{\rho c_C-1}C\}etc][X]}$	(3)

[a)] The symbol $c^{\varnothing}$ stands for the concentration unit in order to make sure that the equilibrium constants are dimensionless.
[b)] We write the equilibria only for the first reaction.

as a linear combination of Langmuir isotherms and that such a linear combination has never the shape of the original Langmuir isotherm. This was used successfully e.g. for analyzing exchange isotherms of sodium and of potassium zeolite A with silver ions [20]. It is therefore interesting to apply the thermodynamic multiple equilibria description with respect to the adsorption of gases with focus on the low relative pressure range where the binding strength between adsorptive and adsorbents is not disturbed by other interactions. This allows to accurately determine the adsorption enthalpy. The entropy evolution is described using the particle distribution theory which holds for adsorbents consisting of materials bearing one or several type of sites and applies for the condition that the adsorptive-adsorbent binding strength is larger than the adsorptive-adsorbate binding strength, so that monolayer coverage is favored. This is equivalent to the condition that the binding enthalpy of the species is the same within each type of sites and independent of those species that are already bonded, which is the Langmuir condition Lc. The meaning of this can be illustrated using a Monte Carlo simulation regarding the occupation of equally distributed adsorption sites as shown in Fig. 1 for 10%, 25%, 50%, and 75% coverage. The simulation is based on the Lc which holds well at low coverage but may become a less good description at larger coverage. Applications regarding argon and nitrogen adsorption isotherms of nonporous, microporous, and mesoporous materials allow comparing systems for which the properties of the active surface span a large range.

1.1. Multiple equilibria

We consider a system in equilibrium consisting of different types of sites $\{n_AA\}$, $\{n_BB\}$, $\{n_CC\}$ etc. where n_A, n_B, n_C etc. denote the number of binding places of the corresponding sites. The equilibria with a ligand or adsorptive *X* can thus be expressed as reported in Table 1. The symbols rc_A, rc_B, rc_C etc. denote the numbers of *X* bound to the corresponding type of site, with $rc_A = 0,1, \ldots,n_A$; $rc_B = 0,1, \ldots,n_B$; $rc_C = 0,1, \ldots,n_C$ etc. and we use $\rho c_A = 1,2, \ldots,n_A$; $\rho c_B = 1,2, \ldots,n_B$; $\rho c_C = 1,2, \ldots,n_C$ etc. to distinguish the equilibria. The large number of individual equilibrium reactions is difficult if not impossible to handle. We therefore adapt the results reported in refs. [19,20] to adsorption processes and we show that the large number of equilibria can be reduced because of the Lc, which as a consequence allows applying the particle distribution function and hence to evaluate the entropy evolution with increasing coverage. More importantly we find that this leads to Langmuir's equation for each site independently and that the total fractional amount of bound *X* can be expressed by means of the linear combination of Langmuir functions.

1.2. Experimental data

We apply this theory to adsorption isotherms of silica particles prepared by the Stöber process, of potassium Zeolite L (ZL), and of potassium ZL containing Indigo (Indigo-ZL) within its channels, and to adsorption isotherms of 3 types of mesoporous silica (MCM-41) [21] adsorbents. The argon isotherms and a short characterization of the adsorbents are shown in Fig. 2 as a plot of the adsorbed volume of gas V_{ads} versus the relative pressure p_{rel} defined in eqn (4), where p is the experimental pressure and p_0 is the saturation pressure of the gas at the experimental temperature. Nitrogen adsorption isotherms are reported in Fig. SI1.

$$p_{rel} = \frac{p}{p_0} \tag{4}$$

The inflection points are inscribed by means of vertical lines. They mark the point where the curvature changes sign and were therefore determined by numerically evaluating the second derivatives which vanish at this point, according to eqn (5).

$$\frac{d^2}{dp_{rel}^2} V_{ads} = 0 \tag{5}$$

The semilog plot in Fig. 2(C), (C′), and (C′′) emphasizes the differences of the curves at low pressure. The importance of showing isotherms as semilog plot, especially in the low relative pressure range, has been pointed out by several authors [20,22]. Stöber type silica particles are well-known for their almost perfect spherical morphology, their low polydispersity, Fig. 2(A), and as excellent non-porous reference materials for the investigation of adsorption processes involving micro- and mesoporous adsorbents [23,24]. Assuming an uniform particle diameter of 375 nm, a bulk density of 1.9 g/cm^3 [23] and perfect spherical morphology without surface roughness leads to a geometric surface area of 8.4 m^2/g. ZL [25], Fig. 2(A′), is a material consisting of linear

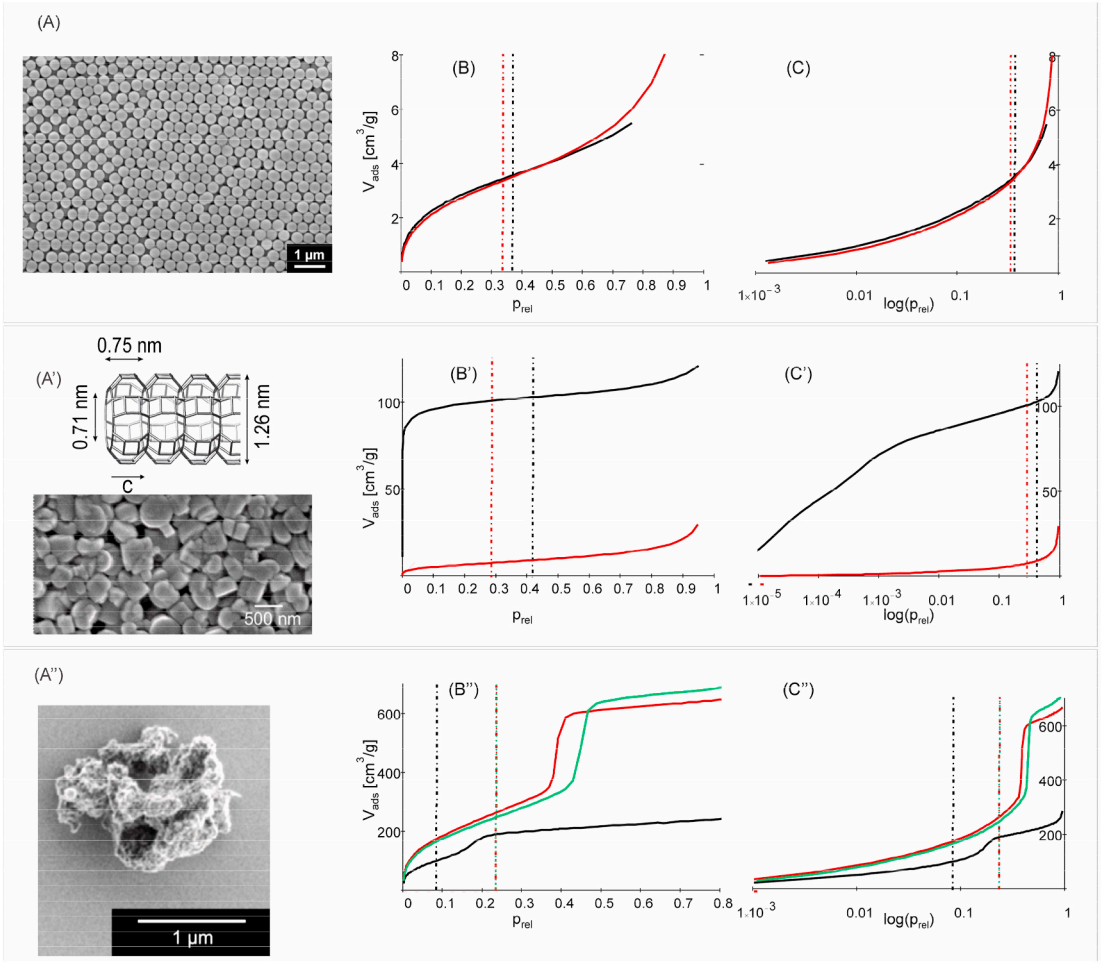

Fig. 2. Experimental Ar adsorption isotherms of nonporous (A), microporous (A′), and mesoporous (A′′) adsorbents. The volume adsorbed V_{ads} as a function of the relative pressure p_{rel} is shown. (A) SEM image of the investigated Stöber-type silica particles. (B) Isotherm measured at 77 K (black) and at 87 K (red). (A′) SEM image of a ZL sample and illustration of a channel [26]. (B′) Isotherm measured at 87 K of ZL (black) and of Indigo-ZL (red). (A′′) Representative SEM image of a MCM-41 particle [42]. (B′′) Isotherm measured at 87 K of MCM-41(2.7 nm) (black), of MCM-41(4.1 nm) (red) and of MCM-41(4.4 nm) (green). (C), (C′), and (C′′) are the semilog plots of the data shown in (B), (B′), and (B′′), respectively. The positions of the numerically determined inflection points are shown as vertical dash-dot lines of the corresponding color. (For interpretation of the references to color in this figure legend, the reader is referred to the Web version of this article.)

channels of about 1 nm diameter which has been investigated in a surprisingly broad field of applications, ranging from catalysis, lubricant technology, pigments, sensing, optoelectronics, biology and even human medicine [26]. The structure, morphology, and the numerous applications of MCM-41 type materials, Fig. 2(A′′), have been reported e.g. in refs [27–30]. The different properties, and especially the different active surface, which ranges from about 10 m^2/g to nearly 10^3 m^2/g, are well reflected by the isotherms in Fig. 2 (Fig. SI1). The numerically determined inflection point marks the region above which new interactions come into play and where we definitely leave the low relative pressure range we are interested in. A theoretical inflection point can be determined using the BET theory designed by Brunauer, Emmett and Teller to describe the adsorption of gases in multimolecular layers [31] which for the first time explained the often observed S-shape of adsorption isotherms. It reduces in its limiting case to Langmuir's equation. It was recommended by the authors for relative pressures p_{rel} larger than approximately 0.05 because it fails at very low p_{rel}. Authoritative reviews and comments regarding the adsorption of gases have been published [32–37]. BET theory, which is widely used in the surface characterization of a variety of solids, e.g. catalysts [38], metal-organic frameworks [39], materials with complex pore systems [40], or environmental nanoparticles [41], provides information on the specific surface area of the adsorbent, the average heat of adsorption of the first layer, and the critical pressure for monolayer coverage [31]. We will use it, where appropriate, for comparison. Based on the multiple equilibria description mentioned above [20] and suggestions going back to Langmuir [1] we have revisited the low relative pressure range. Analysis of multiple equilibria of compounds with different sites is extended to the description of adsorption isotherms. The entropy evolution is described using the particle distribution theory which also holds for adsorbents consisting of materials bearing more than one type of sites as reported in Table 1. No assumption concerning the growth mechanism and specifics regarding the structure of the surface is needed. We find on a rigorous basis that this leads to Langmuir's equation for each site independently, that the total fractional amount of bound adsorptive can be described as a linear combination of individual Langmuir isotherms, and that such a linear combination has never the shape of the original Langmuir isotherms. The results are successfully applied to the argon and nitrogen adsorption isotherms of nonporous, microporous, and mesoporous materials reported in Fig. 2 and in Fig. SI1. The description in terms of multiple equilibria provides a sound basis for improving atomistic understanding. Our results allow to characterize the most active sites, which are the first to be occupied at low relative pressure, and to determine the corresponding adsorption enthalpy. This leads to more accurate data for the specific surface area and for the volume of the gas adsorbed upon formation of a monolayer. This is important because the

surface properties of such materials play a major role in adsorption, catalysis, drug delivery, and separation.

2. Experimental

Chemicals. Aqueous ammonia (ACS reagent, 28.0–30.0% NH_3), ethanol (puriss. p.a., ACS reagent, 96%), tetraethyl orthosilicate (TEOS, reagent grade, ≥ 98%), decyltrimethylammonium bromide (DTAB, ≥98.0%), hexadecyltrimethylammonium bromide (CTAB, ≥98%), and octadecyltrimethylammonium bromide (ODTAB, 98%) were purchased from Sigma-Aldrich and used without further purification.

Synthesis of Stöber-type silica particles. Aqueous ammonia (14.0 mL), ethanol (50.5 mL), and deionized H_2O (43.0 mL) were mixed for 10 min in a 250 mL polypropylene beaker. TEOS (12 mL, 54 mmol) was added to the solution under strong magnetic stirring (approx. 600 rpm). A watch glass was placed over the top of the reaction vessel and the turbid mixture was left to stir. After 4 h the product was divided into two 50 mL centrifuge tubes and centrifuged at 4000 rpm for 20 min. The resulting particles were washed three times with deionized H_2O (30 mL) and once with ethanol (30 mL). The particles were then left to dry at 80 °C overnight and calcined at 550 °C for 5 h with a heating rate of 1 K/min.

Potassium Zeolite L (ZL) and potassium Indigo-Zeolite L (Indigo-ZL). Synthesis and a description of these materials are reported in ref. [43].

MCM-41. The MCM-41 type materials were synthesized as follows [44]. CTAB (2.20 g, 6.04 mmol) (or DTAB (1.69 g, 6.03 mmol) or ODTAB (2.37 g, 6.04 mmol)) was dissolved at 35 °C in a solution of water (53 mL) and aqueous ammonia (25 mL). Once fully dissolved under magnetic stirring, the solution was allowed to cool to room temperature before TEOS (10 mL) was added dropwise. Agitation was continued for 3 h at room temperature. The suspension was then transferred into a Teflon-lined autoclave, which was placed in a pre-heated oven (110 °C). After 48 h, the autoclave was removed from the oven and allowed to cool to room temperature. The product was filtered and washed with 1 L of water with the aid of vacuum filtration. After the product was dried in an oven set to 80 °C for 2 h, the organic surfactant was removed through calcination (300 °C, 2 h followed by 550 °C for 16 h, heating rate of 1 K/min).

Physical measurements. Prior to sorption measurements, the samples were vacuum-degassed at 150 °C for 3 h. The adsorption isotherms were measured with a Quantachrome Autosorb iQ MP. A CryoCooler was used for the measurement of argon adsorption at 87 K. Measurements at 77 K were conducted by cooling with a liquid nitrogen bath. The saturation vapor pressure p_0 was experimentally determined during the measurements. The adsorption isotherms were measured with high resolution in the low relative pressure range (58 points below $p/p_0 = 0.4$). Scanning electron microscopy (SEM) images were obtained with a Quanta FEG 250. The samples were gold coated before SEM images were taken.

Data analysis. The Levenberg-Marquardt method [45,46] was used for the numerical evaluation of the experimental data and to determine the parameters. The acceptance criteria are residuals of up to ±1% and mean square error of less than 0.1. Monte Carlo simulations were performed as reported in ref. [47]. The statistical error of the data is in all cases such that the last digit is significant.

3. Theory

We consider the chemical equilibria in Table 1 to briefly explain the analysis of multiple equilibria of compounds with different sites, with emphasis on adsorption processes. The number of distinguishable chemical objects $\{X_{rc_A}A\}\{X_{rc_B}B\}\{X_{rc_C}C\}etc$ is equal to $(n_A+1)(n_B+1)(n_C+1)\ldots$ and the number of equilibria with X is $(n_A+1)(n_B+1)(n_C+1)\ldots -1$ which is also the number of equilibrium constants. These numbers are so large that they can usually not be handled. It can be shown that the particle distribution theory, which applies for systems where the Lc holds, allows to express the $[(n_A+1)(n_B+1)(n_C+1)\ldots -1]$ equilibrium constants as a function of a number of constants that is equal to the number of different types of binding sites. We consider the ratio of the equilibrium constants in order to find this result. It is therefore useful to extend the notation by using $r_A = 1,2,\ldots,n_A\text{-}1$; $r_B = 1,2,\ldots,n_B\text{-}1$; $r_C = 1,2,\ldots,n_C\text{-}1$ and so on. The ratios of the equilibrium constants between two successive reactions r_A, r_A+1, and r_B, r_B+1, and r_C, r_C+1 and so on are expressed in eqns (6)–(8).

$$\frac{K^{A}_{r_A,r_B,r_C\ldots}}{K^{A}_{r_A+1,r_B,r_C\ldots}} = \frac{[\{X_{r_A}A\}\{X_{r_B}B\}\{X_{r_C}C\}etc\,]^2}{[\{X_{r_A-1}A\}\{X_{r_B}B\}\{X_{r_C}C\}etc][\{X_{r_A+1}A\}\{X_{r_B}B\}\{X_{r_C}C\}etc]} \tag{6}$$

$$\frac{K^{B}_{r_{c_A},r_B,r_C\ldots}}{K^{B}_{r_{c_A},r_B+1,r_C\ldots}} = \frac{[\{X_{r_{c_A}}A\}\{X_{r_B}B\}\{X_{r_C}C\}etc\,]^2}{[\{X_{r_{c_A}}A\}\{X_{r_B-1}B\}\{X_{r_C}C\}etc][\{X_{r_{c_A}}A\}\{X_{r_B+1}B\}\{X_{r_C}C\}etc]} \tag{7}$$

$$\frac{K^{C}_{r_{c_A},r_{c_B},r_C\ldots}}{K^{C}_{r_{c_A},r_{c_B},r_C+1\ldots}} = \frac{[\{X_{r_{c_A}}A\}\{X_{r_{c_B}}B\}\{X_{r_C}C\}etc\,]^2}{[\{X_{r_{c_A}}A\}\{X_{r_{c_B}}B\}\{X_{r_C-1}C\}etc][\{X_{r_{c_A}}A\}\{X_{r_{c_B}}B\}\{X_{r_C+1}C\}etc]} \tag{8}$$

It is in the following sufficient to consider only one of these equilibria, because the equations are analogous. We choose the equilibria on sites A. The free reaction enthalpy is expressed in eqn (9), where T is the temperature and R the ideal gas constant.

$$\Delta^{A}_{R}G^{\varnothing}_{r_A,r_{c_B},r_{c_C}\ldots} = \Delta^{A}_{R}H^{\varnothing}_{r_A,r_{c_B},r_{c_C}\ldots} - T\Delta^{A}_{R}S^{\varnothing}_{r_A,r_{c_B},r_{c_C}\ldots} = -RTln\left(K^{A}_{r_A,r_{c_B},r_{c_C}\ldots}\right) \tag{9}$$

This equation can be split into the particle distribution (pd) and all other contributions (oc). The first reaction on sites A serves as a reference by subtracting the free reaction enthalpy $\Delta^{A}_{R}G^{\varnothing}_{1,0,0\ldots}$ and writing

$$\delta^{A}_{R}G^{\varnothing}_{r_A,r_{c_B},r_{c_C}\ldots} = \Delta^{A}_{R}G^{\varnothing}_{r_A,r_{c_B},r_{c_C}\ldots} - \Delta^{A}_{R}G^{\varnothing}_{1,0,0\ldots} \tag{10}$$

The same is applied to the first reaction on all other sites. This is an extension of the procedure reported in ref. 20 and specifies the more general theoretical reasoning to adsorption processes. It leads to eqn (11) and allows detaching the contribution of the particle distribution (pd) term [19,48,49] and, hence, to discuss its consequences separately.

$$\delta^{A}_{R}G^{\varnothing}_{r_A,r_{c_B},r_{c_C}\ldots} = \delta^{A,oc}_{R}G^{\varnothing}_{r_A,r_{c_B},r_{c_C}\ldots} - T\delta^{A,pd}_{R}S^{\varnothing}_{r_A,r_{c_B},r_{c_C}\ldots} = -RTln\frac{K^{A}_{r_A,r_{c_B},r_{c_C}\ldots}}{K^{A}_{1,0,0\ldots}} \tag{11}$$

We express this for the equilibrium constants in eqn (12).

$$ln\frac{K^{A}_{r_A,r_{c_B},r_{c_C}\ldots}}{K^{A}_{1,0,0\ldots}} = ln\frac{K^{A,oc}_{r_A,r_{c_B},r_{c_C}\ldots}}{K^{A,oc}_{1,0,0\ldots}} + ln\frac{K^{A,pd}_{r_A,r_{c_B},r_{c_C}\ldots}}{K^{A,pd}_{1,0,0\ldots}} \tag{12}$$

These equations serve to evaluate the influence of the particle distribution on the value of the equilibrium constants. The activity coefficients cancel in $\frac{K^{A}_{r_A,r_{c_B},r_{c_C}\ldots}}{K^{A}_{1,0,0\ldots}}$ or play a minor role and will therefore not be considered explicitly. The terms $\delta^{A,oc}_{R}G^{\varnothing}_{r_A,r_{c_B},r_{c_C}\ldots}$ vanish, if the binding enthalpy of the species is the same for all binding sites A and independent of the species that are already bonded, which is the Lc. The same holds for all other binding sites. Eqn (11), hence, simplifies as follows.

$$\delta^{A}_{R}G^{\varnothing}_{r_A,r_{c_B},r_{c_C}\ldots} = \delta^{A,pd}_{R}G^{\varnothing}_{r_A,r_{c_B},r_{c_C}\ldots} = -T\delta^{A,pd}_{R}S^{\varnothing}_{r_A,r_{c_B},r_{c_C}\ldots} \tag{13}$$

$$\delta^{A,pd}_{R}G^{\varnothing}_{r_A,r_{c_B},r_{c_C}\ldots} = -RTln\frac{K^{A,pd}_{r_A,r_{c_B},r_{c_C}\ldots}}{K^{A,pd}_{1,0,0\ldots}} \;\textit{and}\; \delta^{A,pd}_{R}S^{\varnothing}_{r_A,r_{c_B},r_{c_C}\ldots} = Rln\frac{K^{A,pd}_{r_A,r_{c_B},r_{c_C}\ldots}}{K^{A,pd}_{1,0,0\ldots}} \tag{14}$$

This provides the means to discuss the ratio of the equilibrium constants in eqns (6)–(8). We apply the separation of the particle distribution term from any other contribution and remember that the oc term

$\ln \frac{K^{\mathrm{A,oc}}_{r_A+1,rc_B,rc_C\ldots}}{K^{\mathrm{A,oc}}_{r_A,rc_B,rc_C\ldots}}$ cancels because of the Lc. Hence, we can write eqn (15).

$$\frac{K^{\mathrm{A}}_{r_A+1,rc_B,rc_C\ldots}}{K^{\mathrm{A}}_{r_A,rc_B,rc_C\ldots}} = \frac{K^{\mathrm{A,pd}}_{r_A+1,rc_B,rc_C\ldots}}{K^{\mathrm{A,pd}}_{r_A,rc_B,rc_C\ldots}} \tag{15}$$

3.1. Entropy decrease

The ratio of the particle distribution term can be used by applying the particle distribution function [19,48,49]. It takes the form expressed in eqn (16) for sites A, and analogous for sites B, C, and so on.

$$\mathrm{f}(n_A, r_A) = \frac{r_A}{r_A+1}\cdot\frac{n_A - r_A}{n_A - r_A + 1} \tag{16}$$

Using this allows us to write:

$$K^{\mathrm{A,pd}}_{r_A+1,rc_B,rc_C\ldots} = K^{\mathrm{A,pd}}_{r_A,rc_B,rc_C\ldots}\mathrm{f}(n_A, r_A) \tag{17}$$

This means that knowing the value of $K^{\mathrm{A,pd}}_{1,rc_B,rc_C\ldots}$ we know all other equilibrium constants. From this follows that we also know the course of the contributions of the particle distribution term to the free reaction enthalpies and we know the evolution of the entropy contribution.

$$\delta^{\mathrm{A,pd}}_{\mathrm{R}}\mathrm{S}^{\varnothing}_{r_A+1,rc_B,rc_C\ldots} = \mathrm{R}\ln\frac{K^{\mathrm{A,pd}}_{r_A+1,rc_B,rc_C\ldots}}{K^{\mathrm{A,pd}}_{1,0,0\ldots}} \tag{18}$$

It is not necessary to know the values of $\Delta^{\mathrm{A,pd}}_{\mathrm{R}}\mathrm{G}^{\varnothing}_{1,0,0\ldots}$ and $\Delta^{\mathrm{A,pd}}_{\mathrm{R}}\mathrm{S}^{\varnothing}_{1,0,0\ldots}$ in order to know the progress with increasing r_A. The same holds for reactions on all other sites. We report in Fig. 3 the decrease of entropy $\delta^{\mathrm{A,pd}}_{\mathrm{R}}\mathrm{S}^{\varnothing}_{r_A,0,0\ldots}$ with progress of adsorption for r_A = 1, 2, …,10^4 and 1, 2, …,2x10^4 and we illustrate the thus resulting decrease of the equilibrium constants. This explains that the advance of the adsorption process is controlled by the decrease of entropy.

The results are in this form not ready for analyzing experimental data. An important consequence of the Lc is that it allows applying the particle distribution function. This is fortunate, because it makes it possible to collect the very large number of individual equilibrium reactions described in Table 1, as we have explained and proven in detail in refs [19,20]. It means that the sites *{n_AA}, {n_BB}, {n_CC}* etc. establish their equilibria independently. This allows writing eqn (19–21).

$$\{X_{rc_A-1}A\} + X \rightleftarrows \{X_{rc_A}A\} \tag{19}$$

$$\{X_{rc_B-1}B\} + X \rightleftarrows \{X_{rc_B}B\} \tag{20}$$

$$\{X_{rc_C-1}C\} + X \rightleftarrows \{X_{rc_C}C\} \tag{21}$$

etc.

3.2. Linear combination of Langmuir functions

We denote the amount of *X* bound to site *A* as fractional amount θ_A, those bound to site *B* as fractional amount θ_B, those bound to site *C* as fractional amount θ_C. We delivered rigorous proof [19] that these fractional amounts can be expressed by means of Langmuir's equation (22) for each site independently with KL_A, KL_B etc. being the respective Langmuir constants and we showed that the total fractional amount of bound ligand $\theta_{A,B,C,etc}$ can be expressed by means of the linear combination (23) [20].

$$\theta_A = \frac{KL_A[X]}{1+KL_A[X]}\ ,\ \theta_B = \frac{KL_B[X]}{1+KL_B[X]}\ ,\ \theta_C = \frac{KL_C[X]}{1+KL_C[X]}\ etc. \tag{22}$$

$$\theta_{A,B,C} = \frac{n_A\theta_A + n_B\theta_B + n_C\theta_C + etc}{n_A + n_B + n_C + etc} \tag{23}$$

This is the basis of the investigation regarding the adsorption isotherms presented. The situation where a linear combination of two Langmuir isotherms is adequate for describing the data deserves special attention. The empirical justification is that all 18 investigated adsorption isotherms can be very well described in the same way, namely by means of the linear combination of 2 isotherms, Eq. (24) as we will see. Our observation coincides with observations reported in refs. [2–18]. It expresses situations where it is sufficient to distinguish between sites 1 and sites 2, which are characterized by different adsorption enthalpies. The condition is not, that all sites 1 are identical, but it means that the distribution in binding strength is sufficiently narrow, so that we can consider them as being equal within the experimental resolution. The same applies for sites 2. We therefore write eqn (24) in order to express the volume adsorbed V_{ads} as a function of the relative pressure p_{rel}. We refer to this equation as lc2-L (linear combination of 2 Langmuir functions).

$$V_{ads} = a_1\frac{KL'_1 p_{rel}}{1+KL'_1 p_{rel}} + a_2\frac{KL'_2 p_{rel}}{1+KL'_2 p_{rel}} \tag{24}$$

The parameters a_1 and a_2 express the amount of adsorptive adsorbed on sites 1 and on sites 2, respectively. Knowing the relative pressure at which a fractional coverage $\theta_{1,2}$ is established is important. We express this in eqn (25) where V_{mL} is equal to the theoretical volume adsorbed at infinite p_{rel}, which means that V_{mL} is equal to the sum a_1 plus a_2, eqn (26). In order to express the relative pressure p_{rel} as a function of the fractional coverage $\theta_{1,2}$ we need to solve eqn (25):

$$a_1\frac{KL'_1 p_{rel}}{1+KL'_1 p_{rel}} + a_2\frac{KL'_2 p_{rel}}{1+KL'_2 p_{rel}} - \theta_{1,2}V_{mL} = 0 \tag{25}$$

$$V_{mL} = a_1 + a_2 \tag{26}$$

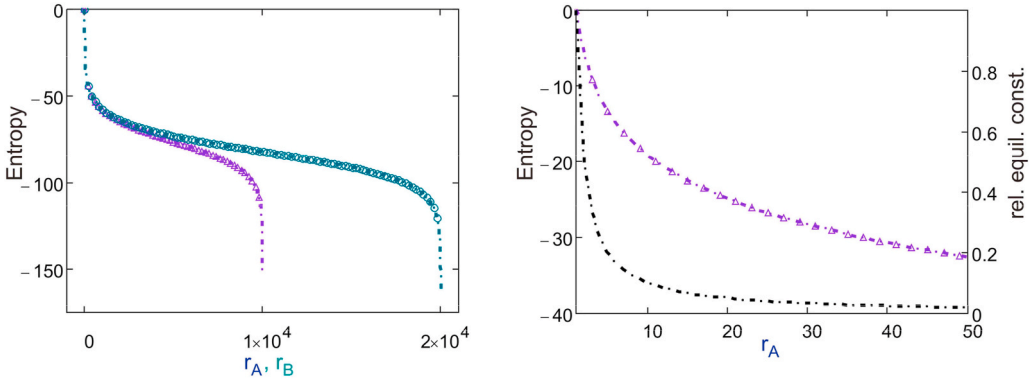

Fig. 3. Decrease of entropy with progress of the adsorption causes a decrease of the equilibrium constant. Left: $\delta^{\mathrm{A,pd}}_{\mathrm{R}}\mathrm{S}^{\varnothing}_{r_A,0,0\ldots}$ [$\mathrm{JK^{-1}mol^{-1}}$] calculated for r_A = 1, 2, …,10^4,(violet) and r_B = 1, 2, …,2x10^4 (green). Right: $\delta^{\mathrm{A,pd}}_{\mathrm{R}}\mathrm{S}^{\varnothing}_{r_A,0,0\ldots}$ [$\mathrm{JK^{-1}mol^{-1}}$] (violet) and relative rate constant $\frac{K^{\mathrm{A}}_{r_A,rc_B,rc_C\ldots}}{K^{\mathrm{A}}_{1,0,0\ldots}}$ (black), shown for r_A = 1, 2, …,50. (For interpretation of the references to color in this figure legend, the reader is referred to the Web version of this article.)

The solution of this equation is expressed in eqn (27)

$$p_{rel} = \frac{-1}{2A}\left[B - \sqrt{B^2 - 4A\Gamma}\right] \tag{27}$$

where the values of A, B and Γ are given by eqn (28)

$$A = \left(1-\theta_{1,2}\right)V_{mL}KL'_1KL'_2 : B = a_1KL'_1 + a_2KL'_2 - \left(KL'_1 + KL'_2\right)V_{mL}\theta_{1,2}\ ,\ \text{and}\ \Gamma = -\theta_{1,2}V_{mL} \tag{28}$$

We know that the upper pressure limit at which the condition for which monolayer coverage is realized must be below the inflection point. We also know that it must be at a fractional coverage $\theta_{1,2}$ smaller than one for adsorption isotherms bearing a shape as seen in Fig. 2 and which is also suggested from the Monte Carlo images reported in Fig. 1. It is, however, as a first guess safe to assume that the condition should be fulfilled up to coverage $\theta_{1,2}$ of about 0.5. This is the value recommended to be used as default, in a first step. It can be confirmed or augmented when analyzing the experimental data. The data analysis process is iterative, because we have only a crude guess for values of KL'_1, KL'_2, a_1, a_2 at the beginning which changes after one or two iteration steps. This means that the numerical analysis is straightforward. The ratio α of the parameters a_1 and a_2, eqn (29) corresponds to the ratio of the amount of adsorptive sites 1 and sites 2, see also eqn (23) of ref. [20].

$$\alpha = \frac{a_1}{a_2} \tag{29}$$

Division of KL'_i, i = 1,2, by the saturation pressure p_0 of the gas delivers the dimensionless thermodynamic constants KL_1 and KL_2, eqn (30), from which the free enthalpy of adsorption and the adsorption enthalpy can be obtained by means of eqns (31) and (32).

$$KL_i = \frac{KL'_i}{p_0} \tag{30}$$

$$\Delta_{ads}G_i^{\varnothing} = -RTln(KL_i) \tag{31}$$

$$\Delta_{ads}H_i^{\varnothing} = \Delta_{ads}G_i^{\varnothing} + T\Delta_{ads}S_i^{\varnothing} \tag{32}$$

The entropy of vaporization measures the entropy increase for the transition of a bound state (for Ar and N_2 of a weakly bound state) to free moving particles (translational and for N_2 also rotational modes) independent of the mechanism. The entropy of adsorption measures the entropy decrease of the reverse process. We can therefore state that the entropy of adsorption of Ar and N_2 at the investigated temperature is equal to the negative value of the entropy of vaporization because the two processes are closely related. This reads as follows:

$$\Delta_{ads}H_i^{\varnothing} \cong \Delta_{ads}G_i^{\varnothing} + T\left(-\Delta_{vap}S_i^{\varnothing}\right) \tag{33}$$

We have now the tools for analyzing the low pressure range where the binding strength between adsorptive and adsorbent is not disturbed by other interactions. This allows to accurately determine the adsorption enthalpy.

4. Results and discussion

We first consider the representation of the low pressure range of the experimental adsorption isotherms reported in Fig. 2 and in Fig. SI1 by means of a Langmuir isotherm eqn (S1). The result is that none of the 8 argon and the 5 nitrogen isotherms we have measured can be described by means of eqn (S1). Fig. 4 illustrates this for three representative examples, namely (A) Stöber-type silica, (B) ZL, and (C) MCM-41 (4.1 nm); see Fig. SI2 for additional examples.

4.1. Application of lc2-L

We will therefore consider a description using the lc2-L eqn (24), including the context reported in eqn (25)–(33). The results of this description are illustrated in Fig. 5 and Table 2 for Ar, and in Fig. 6 and Table 4 for N_2. The figures compare the experimental and the calculated volume adsorbed as a function of the relative pressure p_{rel} and also of the $log(p_{rel})$. Using both representations helps to better grasp the shape of the curves and also to better value the residuals which measure the deviation of the theoretical points from the experimental ones. We observe that all experimental data can accurately be described by means of eqn (24). Experimental points and calculated values can hardly be distinguished. The residuals show that the deviation of the calculated values from the experimental ones is ±1% or less. This means that the low relative pressure regime of the different adsorbents, namely, Stöber-type silica particles, ZL, Indigo-ZL, and the 3 MCM-41(2.7 nm, 4.1 nm, and 4.4 nm) can be well described by means of the lc2-L eqn (24). The latter holds up to the coverage of 0.6. It is interesting that it holds up to nearly complete coverage, namely a value of 0.95, for the ZL adsorbent. The numerically evaluated inflection points illustrated in Fig. 2 are listed in Table 2. They mark the completion of the adsorption process on the bare surface of the adsorbent. This limit is, however, by far not reached in our analysis, as seen in Table 2, where we report for all samples the calculated relative pressure, using eqn (27), at which a

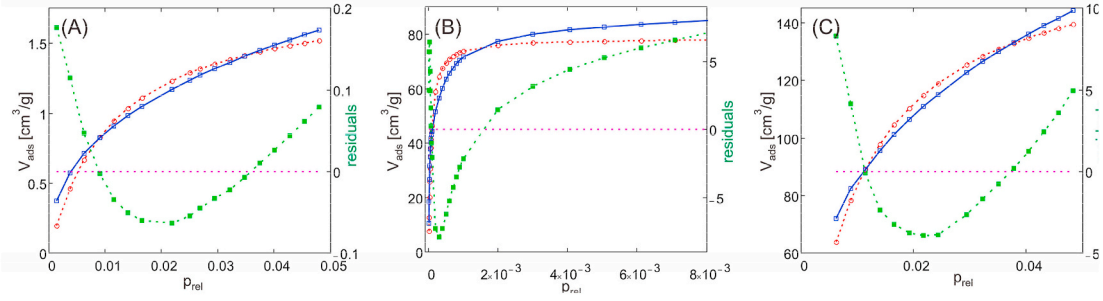

Fig. 4. Comparison of the experimental Ar adsorption isotherms, 87 K, for (A) Stöber-type silica, (B) ZL, (C) MCM-41 (4.1 nm), with the best possible fit using a Langmuir isotherm; eqn (S1). The volume adsorbed as a function of the relative pressure p_{rel} and the residuals are shown. Experimental values: blue lines and squares. Calculated values: red dashed lines and circles. Residuals: green dash-dot lines and squares. (For interpretation of the references to color in this figure legend, the reader is referred to the Web version of this article.)

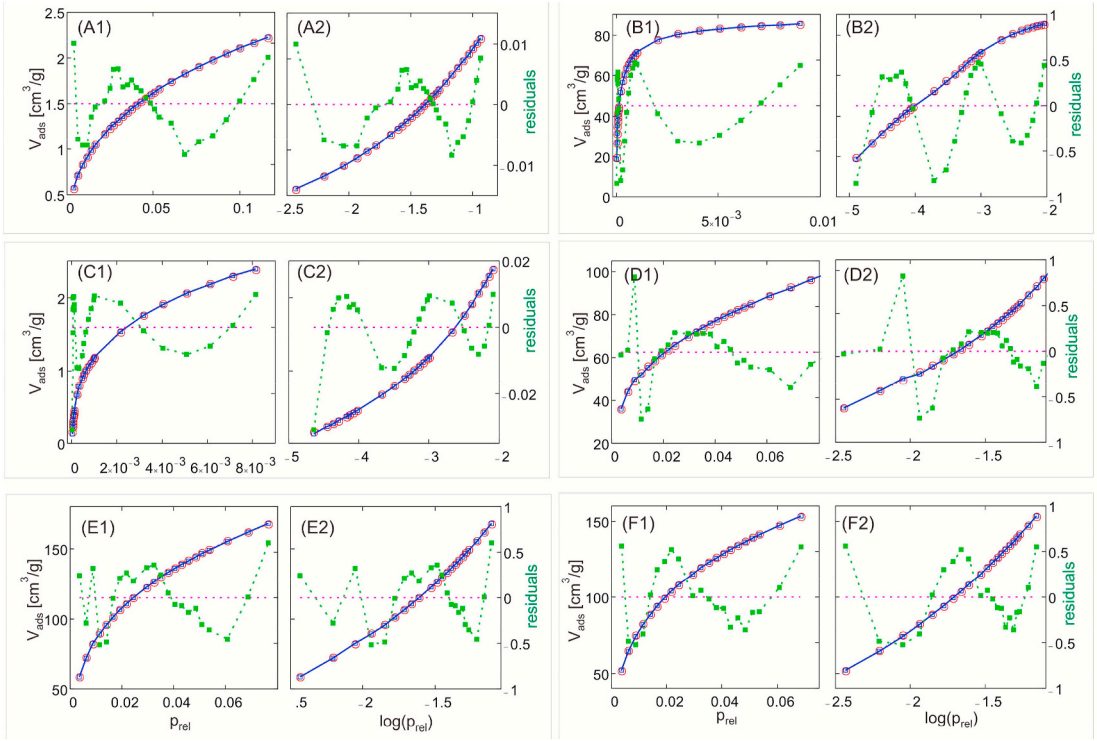

Fig. 5. Comparison of the experimental Ar adsorption isotherms, measured at 87 K, and their description by means of eqn (24). The volume adsorbed is plotted as a function of the relative pressure p_{rel} and of $log(p_{rel})$. The residuals indicate the difference between the experimental and the calculated values. Experimental values: blue lines and squares. Calculated values: red lines and circles. Residuals: green lines and squares. (A1), (A2) Stöber-type silica particles. (B1), (B2) ZL. (C1), (C2) Indigo-ZL. (D1), (D2) MCM-41(2.7 nm). (E1), (E2) MCM-41(4.1 nm). (F1), (F2) MCM-41(4.4 nm). (For interpretation of the references to color in this figure legend, the reader is referred to the Web version of this article.)

Table 2
Results of the Ar (p_0 : 1.069 *bar*, 87*K*) isotherms using eqn (24) in the low pressure range.

Adsorbent	i	a_i[cm^3/g]	KL_i	$\Delta_{ads}G_i^{\varnothing}$ [kJ/mol]	$\Delta_{ads}H_i^{\varnothing}$ [kJ/mol]	$V_{m,Lm}$ [cm^3/g]	A_{Lm} [m^2/g]	0.6 monol. [p_{rel}]	Infl. point [p_{rel}]
Stöber-type silica particles[1)]	1 (1')	0.81 (0.72)	362 (3650)	−4.3 (−5.2)	−11.0 (−11.0)				
	2 (2')	2.97 (2.27)	7.5 (67)	−1.5 (−2.7)	−8.0 (−8.4)				
		α = 0.27 (0.32)				3.7 (3.0)	14 (11)	0.12 (0.053)	0.34 (0.36)
zeolite L[2)]	1	47	48,500	−7.8	−14.3				
	2	40	1490	−5.3	−11.7				
		α = 1.17				88.0	334	2x10^{-4}	0.42
Indigo-ZL	1	0.91	8200	−6.5	−13.0				
	2	2.64	148	−3.6	−10.1				
		α = 0.34				3.5	13.5	5.6x10^{-3}	0.30
MCM-41 (2.7 nm)[3)]	1	49	523	−4.5	−11.0				
	2	133	7	−1.4	−7.8				
		α = 0.37				180	690	0.065[3)]	0.09
MCM-41 (4.1 nm)	1	83	823	−4.4	−10.9				
	2	203	172	−1.6	−8.1				
		α = 0.41				286	1100	0.083	0.24
MCM-41 (4.4 nm)	1	72	375	−4.3	−10.8				
	2	178	12	−1.8	−8.3				
		α = 0.41				251	956	0.065	0.24

[1] Data in parenthesis measured at 77 K, (p_0 : 0.260 *bar*). Data interpreted up to $\theta_{1,2} = 0.6$, with the exceptions of ZL[2)] with $\theta_{1,2} = 0.95$; $p_{rel} = 6x10^{-3}$, and of MCM-41 (2.7 nm)[3)] with $\theta_{1,2} = 0.5$; $p_{rel} = 0.065$.

coverage $\theta_{1,2} = 0.6$ is reached, which serves as a reference. We apply eqn (31) and use the entropy of vaporization $\Delta_{vap}S^{\varnothing}(Ar, 87\ K) = 74.53$ J/(Kmol) [50] to determine the enthalpy of adsorption $\Delta_{ads}H_i^{\varnothing}$ for the sites 1 and 2 according to eqn (33). Table 2 shows that the values of the enthalpy of adsorption $\Delta_{ads}H_i^{\varnothing}$ are in all cases significantly larger or even much larger than the enthalpy of vaporization which amounts to $\Delta_{vap}H^{\varnothing}(Ar, 87\ K) = 6.5$ kJ/mol [50]. This means that the adsorptive-adsorbent binding strength is larger than the adsorptive-adsorbate, so that monolayer coverage is favored in the low relative pressure regime investigated. Because the entropy $\Delta_{ads}S_i^{\varnothing}$ decreases with increasing coverage, however, as illustrated in Fig. 3, the free enthalpy of monolayer adsorption eqn (34) becomes less and less favorable, so that other processes such as formation of clusters and multilayers become dominant at larger coverage.

$$\Delta_{ads}G_i^{\varnothing} = \Delta_{ads}H_i^{\varnothing} - T\Delta_{ads}S_i^{\varnothing} \tag{34}$$

We observe in Table 2 that the enthalpy of adsorption $\Delta_{ads}H_1^{\varnothing}$ for the sites 1 interaction of the Stöber-type silica and of the three MCM-41

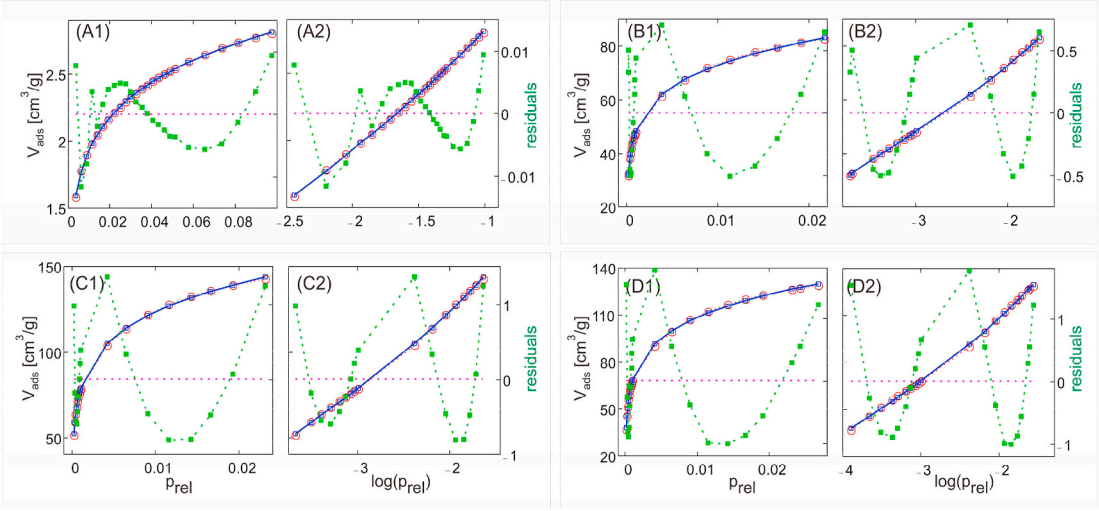

Fig. 6. Comparison of the experimental N_2 adsorption isotherms, measured at 77 K, and their description by means of eqn (24). The volume adsorbed is plotted as a function of the relative pressure p_{rel} and of the $log(p_{rel})$. The residuals indicate the difference between the experimental and the calculated values. Experimental values: blue lines and squares. Calculated values: red lines and circles. Residuals: green lines and squares. (A1), (A2): Stöber-type silica particles. (B1), (B2): MCM-41 (2.7 nm). (C1), (C2): MCM-41(4.1 nm). (D1), (D2): MCM-41(4.4 nm). (For interpretation of the references to color in this figure legend, the reader is referred to the Web version of this article.)

adsorbents are similar, namely about −11 kJ/mol. The situation is analogous for the enthalpy of adsorption $\Delta_{ads}H_2^{\varnothing}$ for the sites 2, which amounts to about −8 kJ/mol. This is remarkable because the specific surface area of the Stöber-type silica and the MCM-41 differs by two orders of magnitude, amounting to 14 m^2/g and about 1000 m^2/g, respectively. The relative amount of site 1 and site 2 interactions is measured by the parameters a_1 and a_2, eqn (24). It is defined with respect to strength of interactions of the adsorptive with the adsorbent. We observe that the number of site 2 interactions dominates. The cross-sectional area of argon is 0.142 nm^2 at 87 K [35,36]. -The situation is different for the ZL where we find a significantly larger enthalpy of adsorption $\Delta_{ads}H_1^{\varnothing}$ for the sites 1 interaction, namely −14.3 kJ/mol, and $\Delta_{ads}H_2^{\varnothing} = -11.7$ kJ/mol for the sites 2. The polar character of the ZL is responsible for the larger adsorptive-adsorbent binding strength [33, 51]. This explains why monolayer coverage behavior is observed up to $\theta_{1,2} = 0.95$. This coverage is already reached at the very low relative pressure $p_{rel} = 6x10^{-3}$. Interestingly, the relative amount of site 1 and site 2 interactions is nearly equal. - The larger adsorptive-adsorbent binding strength, with respect to the Stöber-type silica and the MCM-41 adsorbents, is also present in the Indigo-ZL adsorbent where we find $\Delta_{ads}H_1^{\varnothing} = -13$ kJ/mol and $\Delta_{ads}H_2^{\varnothing} = -10$ kJ/mol. The specific surface area is, however, about 30 times smaller than that of ZL, but nearly equal to that of the Stöber-type silica. The reason is that the indigo molecules partially block the entrance of the channels of the ZL so that essentially only the outer surface of the particles is accessible to the argon adsorptive. As a consequence, the number of site 2 interactions dominates as seen for the Stöber-type silica and the MCM-41 adsorbents.

4.2. BET analysis

Some of these isotherms can be analyzed by means of the BET theory [31] which provides information on the specific surface area A_{BET}, the volume of the gas V_m adsorbed upon formation of a monolayer, and the enthalpy of adsorption. These data can be compared with those reported in Table 2, despite of the fact that the quality of BET representation is less satisfactory as indicated by the shape of the residuals; see Figs. SI3 and SI4. BET also delivers the relative pressure $p_{rel,m}$ at which a monolayer coverage has been reached. The lc2-L description does not provide this information, because monolayer coverage is reached asymptotically. It allows, however, calculating the relative pressure p_{rel} belonging to any desired coverage $\theta_{1,2}$ according to eqn (27). The BET method expresses the volume adsorbed V_{ads} as a function of the relative pressure p_{rel}, eqn (35), where C is a parameter, and it allows to calculate the enthalpy of adsorption $\Delta_{ads}H_{BET}^{\varnothing}$ by means of eqn (36). Eqn (35) is not expected to be valid at low relative pressure smaller than about $p_{rel} \cong 0.05$, as pointed out as a rule by Brunauer, Emmett and Teller [31]. The upper pressure limit at which BET remains valid was analyzed by Rouquerol et al. who found that the product $V_{ads}(1-p_{rel})$ should increase with increasing pressure [34].

$$V_{ads} = V_m C \frac{p_{rel}}{(1-p_{rel})[1+(C-1)p_{rel}]} \tag{35}$$

$$\Delta_{ads}H_{BET}^{\varnothing} = -\left[RTln(C) + \Delta_{vap}H^{\varnothing}\right] \tag{36}$$

Eqn (35) includes the possibility to calculate the inflection point by evaluating the second derivative of V_{ads} with respect to p_{rel}, eqn (5). Evaluating this, see section SI3, we find:

$$-\frac{2CV_m\left(p_{rel}^3(C-1)^2 + p_{rel}(3C-3) - C + 2\right)}{(p_{rel}-1)^3(Cp_{rel}-p_{rel}+1)^3} = 0 \tag{37}$$

This knowledge is used for analyzing the data reported in Fig. 2 by means of BET. We show in Fig. SI3 a comparison of the experimental argon adsorption isotherms and their description by means of the BET eqn (35), and its linearized form eqn (S3) in a similar way as seen in Fig. 5. The comparison of the experimental and the calculated data match the criterion that the deviation should not exceed ±1% for the Stöber-type silica, for the MCM-41(4.1 nm), the MCM-41(4.4 nm), and to a lesser degree for the MCM-41(2.7 nm). The shapes of the experimental and the calculated isotherms of ZL and Indigo-ZL, however, differ considerably. This leads to the conclusion that eqn (35) cannot be applied for these two microporous adsorbents. The numerical results of the BET interpretation are reported in Table 3. We cannot add data for ZL and of Indigo-ZL, for the reasons explained above.

The values for the adsorption enthalpies $\Delta_{ads}H_{BET}^{\varnothing}$ are very similar for the Stöber-type silica and for the three MCM-41 samples. This compares to the lc2-L results in Table 2. We also observe that the BET values are in between those of $\Delta_{ads}H_1^{\varnothing}$ and $\Delta_{ads}H_2^{\varnothing}$. The surface area A_{BET}, and the volume $V_{m,BET}$ of the gas adsorbed upon formation of a monolayer are smaller than those measured using the lc2-L description. This corresponds to what was to be expected, because BET does not describe the

Table 3
Results of the Ar (p_0 : 1.069 *bar*, 87 K) isotherms using the BET eqns (35)–(37).

Adsorbent	RTln(C) [kJ/mol]	$\Delta_{ads}H^{\varnothing}_{BET}$[kJ/mol]	Infl. points [p_{rel}]		$V_{m,BET}$ [cm^3/g]	A_{BET} [m^2/g]	Monolayer [$p_{rel,m}$]
			exp.	theor			
Stöber-type silica particles [a]	2.52	−9.0	0.34	0.22 (0.22)	2.44	9.3	0.16
	(2.33)	(−8.8)	(0.36)		(2.51)	(9.3)	(0.14)
ZL	—	—	0.42	—	—	—	—
Indigo-ZL	—	—	0.30	—	—	—	—
MCM-41 (2.7 nm)	2.8	−9.4	0.09	0.20	110	416	0.12
MCM-41 (4.1 nm)	2.8	−9.3	0.24	0.20	195	742	0.13
MCM-41 (4.4 nm)	2.8	−9.3	0.24	0.20	188	715	0.13

[a] Data in parenthesis measured at 77K; (p_0 : 0.260 *bar*)

low pressure range $p_{rel} < 0.05$ at which the first adsorbate coverage takes place. The relative pressure at which the theoretical inflection point is calculated is much too low for Stöber-type silica and also too low for MCM-41(4.1 nm) and MCM-41(4.4 nm). It is completely wrong for the MCM-41(2.7 nm), which comes not as a surprise if we consider the shape of the corresponding isotherm in Fig. 2(B''), black line. It is difficult to value the relative pressure $p_{rel,m}$ at which BET predicts monolayer coverage. We can compare it with data reported for 60% coverage in Table 2.

4.3. Analysis of the nitrogen adsorption isotherms

The enthalpy of vaporization of N_2 is smaller than that of Ar [52]. It amounts to $\Delta_{vap}H^{\varnothing}(N_2, 77\,K) = 5.58$ kJ/mol [50]. The entropy of vaporization is $\Delta_{vap}S^{\varnothing}(N_2, 77\,K) = 75.22$ J/(Kmol) [50], and thus slightly larger than that of Ar. The consequence is that the condition that the adsorptive-adsorbent binding strength is larger than other interactions is expected to hold up to a larger coverage for N_2 than for Ar. We can test this by analyzing the N_2 adsorption isotherms for the Stöber-type and the MCM-41 adsorbents reported in Fig. SI1. We should add that a description of these isotherms with one Langmuir isotherm, eqn (S1), fails similarly as for Ar as adsorptive, see Fig. SI2. Fig. 6 shows the experimental and calculated volume adsorbed as a function of the relative pressure p_{rel} and also of the $log(p_{rel})$. Eqn (24), including the context reported in eqn (25)–(33), was used in this analysis, as previously done for the argon data. We observe that all experimental data can accurately be described by means of eqn (24). The residuals show that the deviation of the calculated values from the experimental ones is ±1% or less. This means that the low relative pressure regime of the Stöber-type silica particles and of the three MCM-41(2.7 nm, 4.1 nm, and 4.4 nm) adsorbents can be well described by means of the lc2-L eqn (24). The latter holds up to coverage of about $\theta_{1,2} = 0.85$. This value is significantly higher than that observed for Ar. The N_2 adsorption enthalpies $\Delta_{ads}H^{\varnothing}_1$ and $\Delta_{ads}H^{\varnothing}_2$ are slightly smaller for the Stöber-type particles but larger for the MCM-41 adsorbents and compared to those observed for Ar. The result is that the MCM-41 values are about 10% larger. It is interesting, that the surface area A_{Lm}, and the volume of the gas $V_{m,Lm}$ adsorbed upon formation of a monolayer are about 1/3 smaller than those determined with argon as adsorptive. The cross sectional area for Ar is smaller, it amounts to 0.142 nm^2 (at 87 K) and 0.138 nm^2 (at 77 K) [35,36], while that of N_2 is 0.162 nm^2 (at 77 K) [35–37]. We again observe that A_{Lm} and $V_{m,Lm}$ are smaller for the MCM-41(2.7 nm) than those for MCM-41(4.1 nm) and MCM-41(4.4 nm) which are of similar value, but those for MCM-41(4.1 nm) are again the largest. We note that the contribution of site 1 adsorption is larger for N_2 than for Ar.

We can compare the data reported in Table 4 with results using the BET description reported in Table 5. Fig. SI4 shows a comparison of the experimental and the calculated volume adsorbed as a function of the relative pressure p_{rel}. The representation is not satisfactory for the MCM-41(2.7 nm, 4.1 nm and 4.4 nm), but acceptable, similar as we have seen for the Ar isotherms. Again we observe that the values for the adsorption enthalpies $\Delta_{ads}H^{\varnothing}_{BET}$ are very similar for the Stöber-type silica and for the three MCM-41 samples. It is interesting to observe that the value closely matches those of $\Delta_{ads}H^{\varnothing}_2$ (Table 4). The surface area A_{BET}, and the volume of the gas $V_{m,BET}$ adsorbed upon formation of a monolayer are of similar values but smaller. The relative pressure at which the theoretical inflection point is calculated is too low but completely wrong for the MCM-41(2.7 nm), as already seen for argon as adsorptive.

4.4. Evolution of the coverage of sites 1 and sites 2

The new information provided by the lc2-L description allows calculating the evolution of the coverage of sites 1 and sites 2 as a function of increasing pressure. It is convenient to use the simplified notations in eqn (38–40) for expressing the adsorption equilibria.

$$\{S1\} + X \rightleftarrows \{S1\}X\ ,\ KL_1 \tag{38}$$

$$\{S2\} + X \rightleftarrows \{S2\}X\ ,\ KL_2 \tag{39}$$

Table 4
Results of the N_2 (p_0 : 0.983 *bar*, 77 *K*) isotherms using the lc2-L eqn (24) in the low pressure range.[a]

Adsorbent	i	a_i[cm^3/g]	KL_i	$\Delta_{ads}G^{\varnothing}_i$ [kJ/mol]	$\Delta_{ads}H^{\varnothing}_i$ [kJ/mol]	$V_{m,Lm}$ [cm^3/g]	A_{Lm} [m^2/g]	0.6 monol. [p_{rel}]	Infl. point [p_{rel}]
Stöber-type silica particles	1	1.7	2000	−4.9	−10.7				
	2	1.6	23.0	−2.0	−7.8				
		α = 1.1				3.3	14.0	0.012	0.290
MCM-41 (2.7 nm)	1	47.1	9880	−5.9	−11.7				
	2	50.0	113	−3.0	−8.8				
		α = 0.94				97	423	3 x10^{-3}	0.075
MCM-41 (4.1 nm)	1	77.8	8350	−5.8	−11.6				
	2	91.1	111	−3.0	−8.8				
		α = 0.85				169	735	3.7x10^{-3}	0.209
MCM-41 (4.4 nm)	1	66.3	9260	−5.8	−11.6				
	2	85.0	107	−3.0	−8.8				
		α = 0.78				151	659	4.2x10^{-3}	0.218

[a] Data interpreted up to $\theta_{1,2} = 0.85$.

Table 5
Results of the N_2 (p_0 : 0.983 *bar*, 77 K) isotherms using the BET eqns (35)–(37).

Adsorbent	RTln(C) [kJ/mol]	$\Delta_{ads}H^{\varnothing}_{BET}$[kJ/mol]	Infl. points [p_{rel}]		$V_{m,BET}$ [cm^3/g]	A_{BET} [m^2/g]	Monolayer [$p_{rel,m}$]
			exp.	theor.			
Stöber-type silica particles	3.37	−8.96	0.29	0.14	2.7	12.0	0.07
MCM-41 (2.7 nm)	2.98	−8.57	0.075	0.167	109	473	0.09
MCM-41 (4.1 nm)	3.04	−8.63	0.21	0.164	185	803	0.08
MCM-41 (4.4 nm)	3.04	−8.63	0.22	0.164	162	706	0.08

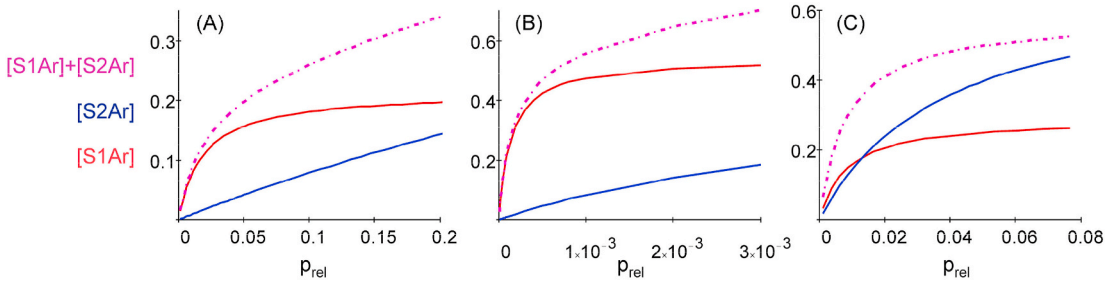

Fig. 7. Evolution of the concentration *[S1Ar]*, red line, of *[S2Ar]*, blue line, and of the sum of both, pink dash-dot as a function of the relative Ar pressure p_{rel} in the range of $\theta_{12} = 0$ to $\theta_{12} = 0.6$. The concentration units are chosen with respect to $C_0 = 1$ for total monolayer coverage. (A) Stöber-type silica particles, (B) ZL, and (C) MCM-41(4.1 nm). (For interpretation of the references to color in this figure legend, the reader is referred to the Web version of this article.)

The concentrations [S1X] and [S2X] of the situations {S1}X and {S2}X are expressed in eqn (40), the derivation of which is explained in section SI5.

$$[\mathrm{S1X}] = \frac{KL_1 C_0 \frac{\alpha \cdot \frac{[X]}{c^{\varnothing}}}{1+\alpha \cdot \frac{[X]}{c^{\varnothing}}}}{1 + KL_1 \frac{[X]}{c^{\varnothing}}} \quad \textit{and} \quad [\mathrm{S2X}] = \frac{KL_2 C_0 \frac{1 \cdot \frac{[X]}{c^{\varnothing}}}{1+\alpha \cdot \frac{[X]}{c^{\varnothing}}}}{1 + KL_2 \frac{[X]}{c^{\varnothing}}} \tag{40}$$

The symbol $c^{\varnothing}$ stands for the concentration unit and C_0 expresses the total concentration of $\{S1\} + \{S2\}$ divided by $c^{\varnothing}$. Eqn (40) allows calculating the evolution of the concentration of sites which have bound a ligand *X*. We use the ideal gas equation [X] = p/RT to calculate the data in Fig. 7, where we show the evolution of the concentrations for the three Ar isotherms for the adsorbents Stöber-type silica particles, ZL, and MCM-41(4.1 nm) as examples. It is interesting to observe, that the evolution of the concentrations of [S1X] and of [S2X] is characteristically different for the three adsorbents. The difference of the free enthalpy of binding (adsorption) suggests that it should be possible to distinguish between [S1X] and [S2X] using a vibrational spectroscopy method such as Raman or far IR.

A way to visualize the equilibria (38), (39) is presented in Fig. 8. The sites {S1} and {S2} are occupied according to their number and their relative affinity depending on the number of adsorptive atoms or molecules, expressed by the equilibrium constants KL_1 and KL_2, respectively. The figure illustrates that the binding strength is not influenced by the number of positions that are occupied. The entropy, however, decreases with increasing occupation in the way reported in Fig. 2. Fig. 8 which illustrates the steps in the formation of two site monolayer adsorption equilibria serves also as guideline for formulating the kinetics of the adsorption process.

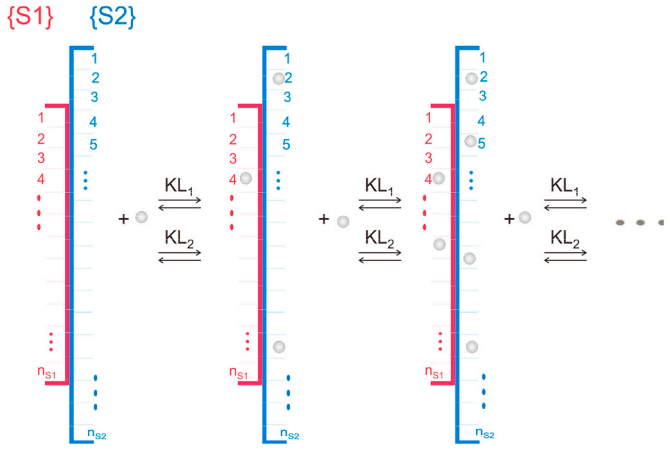

Fig. 8. Scheme of the steps in the formation of two site monolayer adsorption equilibria.

5. Conclusions

It took some time before Langmuir's hypothesis expressed intuitively in the chapter "More than One Kind of Elementary Space" of his 1918 publication, ref. [1], which reads as follows "since each of the different kinds of elementary spaces affects the adsorption independently, the result is the same as if the total surface were divided into certain fractions, β_1, β_2, etc." was discussed and, as a consequence, used successfully to describe systems consisting of several sites with different ease of adsorption and for multi-component gas analysis. Analysis procedures which follow this idea are often abbreviated as DSL for dual-site Langmuir or DPL for dual-process Langmuir [2–18]. We have extended the analysis of multiple equilibria of compounds with different coordination sites to the description of adsorption isotherms with focus on the low pressure range which means to conditions where the adsorptive-adsorbent binding strength is larger than the adsorptive-adsorbate, so that monolayer coverage is favored. It is well established that generally different sites for adsorption of atoms and molecules play a role, characterized by more than one equilibrium reaction [20–22,53–56]. No assumption concerning the growth mechanism and specifics regarding the structure of the surface is needed. The free reaction enthalpy in multiple equilibria can therefore be split into the particle distribution term and all other contributions for each type of sites separately. This allows to evaluate the entropy contribution [19, 20]. The course of the entropy decrease with progress of adsorption is illustrated in Fig. 3. We find on a rigorous basis that this leads to Langmuir's equation for each site independently, that the total fractional amount of bound adsorptive can be described as a linear combination of individual Langmuir isotherms, and that such a linear combination has never the shape of the original Langmuir isotherms thus setting Langmuir's intuitive hypothesis mentioned above on a firm

theoretical base. This allows to accurately determine the adsorption enthalpy. The results are successfully applied to argon and nitrogen adsorption isotherms of nonporous, microporous, and mesoporous adsorbents which allows comparing systems for which the properties of the active surface span a large range. We observe that all experimental data can accurately be described by means of a linear combination of two Langmuir isotherms in the low relative pressure range up to coverage of about 60% for Ar as adsorptive and up to coverage of 85% for N_2. The two site interactions involved exhibit substantially different adsorption enthalpies. This means that the shape of all adsorption isotherms is essentially determined by the entropy decrease with increasing coverage. Interestingly the Ar enthalpy of adsorption $\Delta_{ads}H_1^{\varnothing}$ for the sites 1 of the Stöber-type silica and of all three MCM-41 adsorbents (with pore size of 2.7 nm, 4.1 nm, and 4.4 nm) investigated are similar, namely about −11 kJ/mol. The situation is analogous for the enthalpy of adsorption $\Delta_{ads}H_2^{\varnothing}$ for the sites 2, which amounts to -8 kJ/mol. This seems to indicate that the sites of interaction are very similar in these materials. A significantly larger enthalpy of adsorption $\Delta_{ads}H_1^{\varnothing}$ for the sites 1, namely −14.3 kJ/mol, and $\Delta_{ads}H_2^{\varnothing} = -11.7$ kJ/mol for the sites 2 is measured for potassium zeolite L. The measured specific surface area for these samples ranges from 14 m^2/g for the Stöber-type silica up to 1100 m^2/g for the MCM-41(4.1 nm) adsorbent. The information provided by the lc2-L analysis allows calculating the evolution of the coverage of site 1 and of site 2 as a function of increasing pressure, thus presenting additional insight. The inflection points of the isotherms were determined by numerically evaluating the second derivatives which vanish at this point. All data of the 18 investigated adsorption isotherms can be described accurately by the same approach and we expect that this holds for many other gas adsorption isotherms where the condition that the adsorptive-adsorbent binding strength is larger than the adsorptive-adsorbate is fulfilled. This constitutes a sound basis for quantum mechanical modeling which provides means for atomistic understanding [56], including the potential influence of porosity on monolayer formation [57]. We conclude that the description in terms of multiple equilibria provides a sound basis for improving our atomistic understanding. Our results allow to characterize the most active sites which are the first to be occupied at low relative pressure and they allow to determine the corresponding adsorption enthalpy. This leads to more accurate data for the specific surface area and for the volume of the gas adsorbed upon formation of a monolayer.

Declaration of competing interest

The authors declare that they have no known competing financial interests or personal relationships that could have appeared to influence the work reported in this paper.

Acknowledgements

This work was supported by the Swiss National Science Foundation (project 200021_172805).

Appendix A. Supplementary data

Supplementary data to this article can be found online at https://doi.org/10.1016/j.micromeso.2020.110744.

We have extended the analysis of multiple equilibria of compounds with different coordination sites to the description of adsorption isotherms with focus on the low relative pressure range which means to conditions where the adsorptive-adsorbent binding strength is larger than the adsorptive-adsorbate binding strength, so that monolayer coverage is favored.

No assumption concerning the growth mechanism and specifics regarding the structure of the surface is needed. We find on a rigorous basis that this leads to Langmuir's equation for each site independently, that the total fractional amount of bound adsorptive can be described as a linear combination of individual Langmuir isotherms, and that such a linear combination has never the shape of the original Langmuir isotherms. The results are applied to argon and nitrogen adsorption isotherms of nonporous, microporous, and mesoporous adsorbents which allows comparing systems for which the properties of the active surface span a large range. Our theory provides information on equilibrium constants for sites of substantially different affinity. All data of the 18 investigated adsorption isotherms can be described accurately by the same approach and we have good reason to expect that this holds for many other gas adsorption isotherms where the above-mentioned condition is fulfilled. This is important for applications and constitutes a sound basis for quantum mechanical modeling which provides means for atomistic understanding, including the potential influence of porosity on monolayer formation.

References

[1] I. Langmuir, J. Am. Chem. Soc. 40 (1918) 1361–1403.
[2] A.L. Myers, AlChE J 29 (4) (1983) 691–693.
[3] R.G. Jordi, D.D. Do, J. Chem. Soc. Faraday Trans. 88 (16) (1992) 2411–2419.
[4] A. Micke, M. Billow, M. Kocirik, P. Struve, J. Phys. Chem. 98 (1994) 12337–12344.
[5] P.M. Mathias, R. Kumar, J.D. Moyer Jr., J.M. Schork, S.R. Srinivasan, S.R. Auvil, O. Talu, Ind. Eng. Chem. Res. 351 (1996) 2477–2483.
[6] L. Song, L.V.C. Rees, J. Chem. Soc. Faraday Trans. 93 (4) (1997) 649–657.
[7] W. Zhu, F. Kapteijn, J.A. Moulijn, Chem. Commun. (1999) 2453–2454.
[8] R. Krishna, T.J.H. Vlugt, B. Smit, Chem. Eng. Sci. 54 (1999) 1751–1757.
[9] T.J.H. Vlugt, R. Krishna, B. Smit, J. Phys. Chem. B 103 (1999) 1102–1118.
[10] W. Zhu, F. Kapteijn, J.A. Moulijn, M.C. den Exter, J.C. Jansen, Langmuir 16 (2000) 3322–3329.
[11] D. Paschek, R. Krishna, Phys. Chem. Chem. Phys. 2 (2000) 2389–2394.
[12] S. Keskin, J. Liu, J. Karl Johnson, D.S. Sholl, Langmuir 24 (2008) 8254–8261.
[13] J.A. Ritter, S.J. Bhadra, A.D. Ebner, Langmuir 27 (2011) 4700–4712.
[14] S.J. Bhadra, A.D. Ebner, J.A. Ritter, Langmuir 28 (2012) 6935–6941.
[15] S. García, J.J. Pis, F. Rubiera, C. Pevida, Langmuir 29 (2013) 6042–6052.
[16] K. Liu, B. Li, Y. Li, X. Li, F. Yang, G. Zeng, Y. Peng, Z. Zhang, G. Li, Z. Shi, S. Feng, D. Song, Chem. Commun. 50 (2014) 5031–5033.
[17] A. Farzaneh, M. Zhou, E. Potapova, Z. Bacsik, L. Ohlin, A. Holmgren, J. Hedlund, M. Grahn, Langmuir 31 (2015) 4887–4894.
[18] H. Swenson, N.P. Stadie, Langmuir 35 (2019) 5409–5426.
[19] G. Calzaferri, Phys. Chem. Chem. Phys. 19 (2017) 10611–10621.
[20] G. Calzaferri, Phys. Chem. Chem. Phys. 20 (2018) 29070–29084.
[21] J.A.S. Costa, R.A. de Jesus, D.O. Santos, J.F. Mano, L.P.C. Romãod, C.M. Paranhos, Microporous Mesoporous Mater. 291 (2020) 109698, https://doi.org/10.1016/j.micromeso.2019.109698.
[22] (a) E.A. Ustinov, D.D. Do, M. Jaroniec, Appl. Surf. Sci. 252 (2005) 548–561; (b) M. Khalfaoui, M.H.V. Baouab, R. Gauthier, A. Ben Lamine, Adsorpt. Sci. Technol. 20 (2002) 17–31.
[23] W. Stöber, A. Fink, E. Bohn, J. Colloid Interface Sci. 26 (1968) 62–69.
[24] S. Li, Q. Wan, Z. Qin, Y. Fu, Y. Gu, Langmuir 31 (2015) 824–832.
[25] (a) Ch Baerlocher, W.M. Meier, D.H. Olson, Atlas of Zeolite Framework Types, fifth ed., Elsevier Amsterd, 2001; (b) International Zeolite Association. http://www.iza-structure.org/databases.
[26] G. Calzaferri, Structure and Bonding, Springer, Berlin, 2020. http://doi-org-443.webvpn.fjmu.edu.cn/10.1007/430_2020_57.
[27] Y. Wan, D. Zhao, Chem. Rev. 107 (2007) 2821–2860.
[28] A. Taguchi, F. Schüth, Microporous Mesoporous Mater. 7 (2005) 1–45.
[29] Ch Argyo, V. Weiss, Ch Bräuchle, Th Bein, Chem. Mater. 26 (2014) 435–451.
[30] F. Hoffmann, M. Cornelius, J. Morell, M. Fröba, Angew. Chem. Int. Ed. 45 (2006) 3216–3251.
[31] S. Brunauer, P.H. Emmett, E. Teller, J. Am. Chem. Soc. 60 (1938) 309–319.
[32] W. Rudzinski, D.H. Everett, Adsorption of Gases on Heterogeneous Surfaces, Academic Press, London, 1992, ISBN 0-12-601690-9.
[33] M.P.L. Llewellyn, G. Maurin, in: J. Cejka, H. Bekkum, A. Corma, F. Schüth (Eds.), Introduction to Zeolite Science and Practice, third ed., Elsevier Amsterdam, 2007, pp. 556–610. Chapter 17.
[34] J. Rouquerol, P. Llewellyn, F. Rouquerol, Stud. Surf. Sci. Catal. 160 (2007) 49–56.
[35] M. Thommes, K. Kaneko, A.V. Neimark, J.P. Olivier, F. Rodriguez-Reinoso, J. Rouquerol, K.S.W. Sing, Pure Appl. Chem. 87 (2015) 1051–1069.
[36] (a) F. Rouquerol, J. Rouquerol, K. Sing, Adsorption by Powders and Porous Solids, Academic Press, London, 1999; (b) K. Sing, Colloids Surf., A 187–188 (2001) 3–9.
[37] T.C. Brown, D.J. Miron, Ch M. Fellows, PhysChemChemPhys 21 (2019) 2558–2566.
[38] G. Leofanti, M. Padovan, G. Tozzola, B. Venturelli, Catal. Today 41 (1998) 207–219.
[39] F. Ambroz, T.J. Macdonald, V. Martis, I.P. Parkin, Small Methods 2 (2018) 1800173.
[40] M.J. Reber, D. Brühwiler, Dalton Trans. 44 (2015) 17960–17967.
[41] D.J. Burleson, M.D. Driessen, R.L. Penn, J. Environ. Sci. Health A 39 (2004) 2707–2753.

[42] Y. Ma, P. Rajendran, Ch Blum, Y. Cesa, N. Gartmann, D. Brühwiler, V. Subramaniam, J. Colloid Interface Sci. 356 (2011) 123–130.
[43] P. Woodtli, S. Giger, P. Müller, L. Sägesser, N. Zucchetto, M.J. Reber, A. Ecker, D. Brühwiler 149 (2018) 456–461.
[44] D. Brühwiler, H. Frei, J. Phys. Chem. B 107 (2003) 8547–8556.
[45] The Levenberg-Marquardt Method Implemented in Mathcad 15, Mathsoft Eng. & Edu., Inc. http://www.mathsoft.com.
[46] D.W. Marquardt, J. Soc. Ind. Appl. Math. 11 (1963) 431–441.
[47] M.M. Yatskou, M. Meyer, S. Huber, M. Pfenniger, G. Calzaferri, ChemPhysChem 4 (2003) 567–587.
[48] (a) A. Kunzmann, R. Seifert, G. Calzaferri, J. Phys. Chem. B 103 (1999) 18–26. Eqn (4) and (31) should read: (4) $\theta_i(r)=N_{r,i}/N_{uc}$ and (31) $logK_a=(a_{Zn}\ a_M)/(a_{ZM}\ a_N)=\cdots$;
(b) M. Meyer, A. Currao, G. Calzaferri, ChemPhysChem 6 (2005) 2167–2178.
[49] (a) K. Baudet, S. Guerra, C. Piguet, Chem. Eur J. 23 (2017) 16787–16798;
(b) G. Ercolani, C. Piguet, M. Borkovec, J. Hamacek, J. Phys. Chem. B 111 (2007) 12195–12203.
[50] P.W. Atkins, J. de Paula, Physikalische Chemie, 4. Auflage, Wiley-VCH Weinheim, 2006, ISBN 3-527-31546-2.
[51] R.M. Barrer, Zeolites and Clay Minerals as Sorbents and Molecular Sieves, Academic Press, London, 1978, 0120793504. Chapter 4.
[52] Due to its quadrupole moment, the orientation of a nitrogen molecule is dependent on the surface chemistry of the adsorbent. This leads to an uncertainty which can reach 20% on some surfaces. The corresponding value for srgon is more reliable.
[53] W.L. Queen, M.R. Hudson, E.D. Bloch, J.A. Mason, M.I. Gonzalez, J.S. Lee, D. Gygi, J.D. Howe, K. Lee, T.A. Darwish, M. James, V.K. Peterson, S.J. Teat, B. Smit, J. B. Neaton, J.R. Long, C.M. Brown, Chem. Sci. 5 (2014) 4569–4581.
[54] X. Han, H.G.W. Godfrey, L. Briggs, A.J. Davies, Y. Cheng, L.L. Daemen, A. M. Sheveleva, F. Tuna, E.J.L. McInnes, J. Sun, C. Drathen, M.W. George, A. J. Ramirez-Cuesta, K.M. Thomas, S. Yang, M. Schröder, Nat. Mater. 17 (2018) 691–696.
[55] C. Deiana, M. Minella, G. Tabacchi, V. Maurino, E. Fois, G. Martra, Phys. Chem. Chem. Phys. 15 (2013) 307–315.
[56] G. Tabacchi, ChemPhysChem 19 (2018) 1249–1297.
[57] L.D. Gelb, K.E. Gubbons, Langmuir 14 (1998) 2097–2111.